Part IV

Nonlinear relaxation dynamics of free surface oscillations due to contact angle hysteresis

Introduction

In Part II, we have tackled several aspects of sloshing, an archetypal resonator system in fluid mechanics which sometimes represents a critical issue in mechanical engineering and daily life. It is therefore crucial to understand its associated damping. Indeed, the latter plays a fundamental role in the mitigation of the wave amplitude response in resonant conditions.

We have mentioned how originally the eigenfrequencies of standing capillary-gravity waves in closed basins were derived in the potential flow limit (Lamb, 1993), while the linear viscous dissipation at the free surface, at the solid walls and in the bulk for low-viscosity fluids was typically accounted for by a boundary layer approximation (Case and Parkinson, 1957; Miles, 1967; Ursell, 1952). This classic theoretical approach, which has been used in Part II, is built on the simplifying assumption that the free liquid surface, η, intersects the lateral wall orthogonally and the contact line can freely slip at a velocity $\partial\eta/\partial t$ ($\sim U$) and with a constant zero slope,

$$\frac{\partial \eta}{\partial n} = 0 \quad \text{free-end edge condition,}$$

where $\partial/\partial n$ is the spatial derivative in the direction normal to the lateral wall. Chapters 4, 5 and 6, have proven these hypotheses reasonable for the modelling of gravity-dominated waves in moderately large-size containers, although some mismatch between theory and experiments is still present. Such a mismatch was partially attributed to additional dissipations sources acting at the moving contact line, whose dynamics is the central topic of this **Part IV**.

The classical assumption of a free-end edge condition has been relaxed in Part III, where two other scenarios have been studied within the framework of the Faraday instability in small-size partially filled containers. In Chapter 7, we have considered a diametrically opposed boundary condition, namely a pinned-end edge, according to which the contact line is fixed,

$$\frac{\partial \eta}{\partial t} = 0 \quad \text{pinned-end edge condition,}$$

while the slope, $\partial\eta/\partial n$, is let free to vary (Benjamin and Scott, 1979; Graham-Eagle, 1983). In this case, theoretical predictions have provided an estimation of the sub-harmonic Faraday threshold in good agreement with experimental measurements. Indeed, with the contact line being fixed, the system's dissipation can be estimated accurately, since no extra and undetermined dissipation is generated by the contact line.

In Chapter 8, the instability onset of Faraday waves in Hele-Shaw cells and with a moving

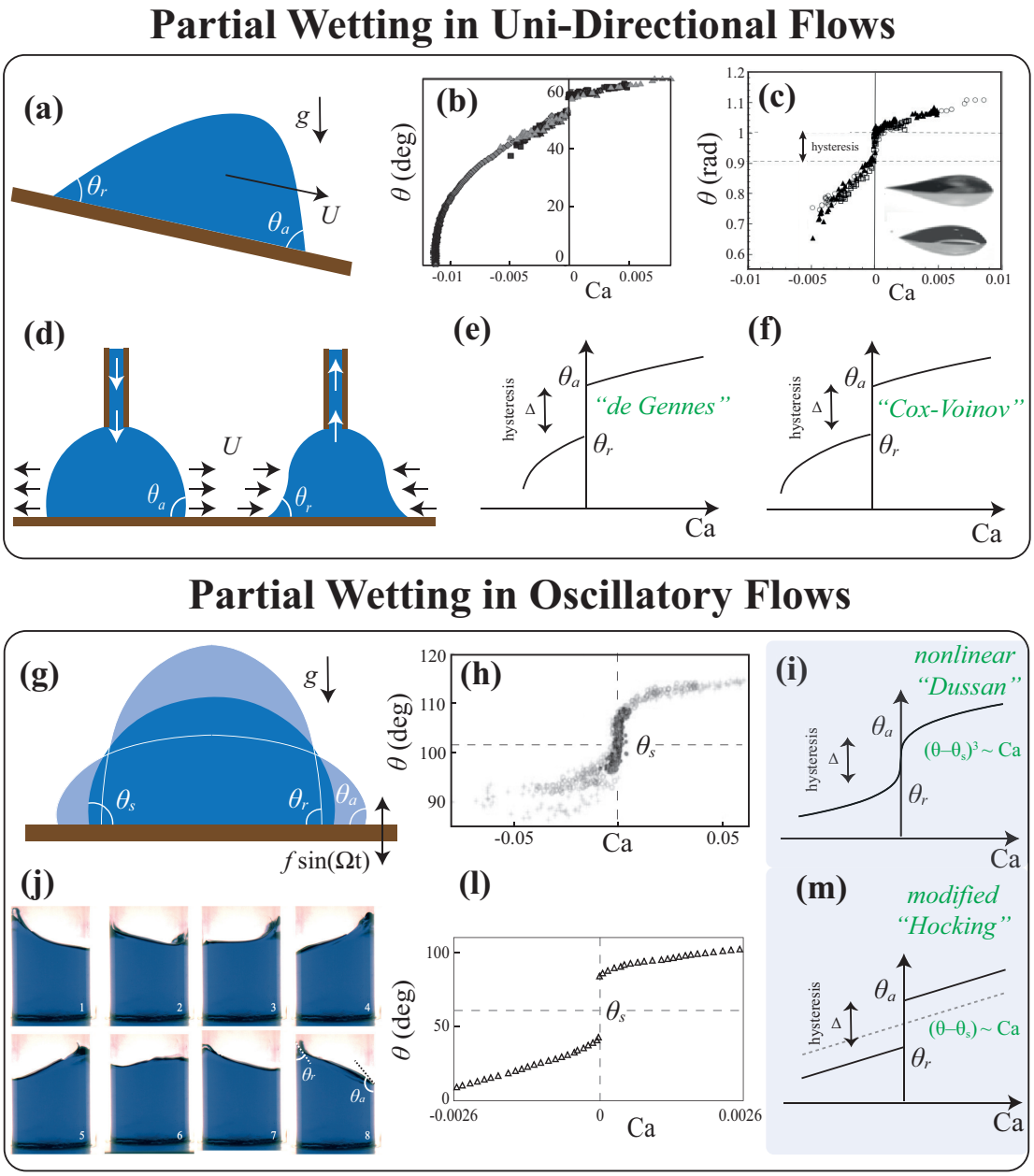

Figure IV.1 – (a) Advancing, θ_a, and receding, θ_r, contact angles in a droplet sliding down with velocity U over a dry substrate (partial wetting). (d) Contact angles in an expanding and contracting liquid droplet. Both (a) and (d) are examples of uni-directional flows. The dynamic contact angle is seen experimentally to depend on the capillary number, $Ca = \mu U/\gamma$, as reported by (b) Snoeijer and Andreotti (2013) and (c) Rio et al. (2005). The dependence of the contact angle, θ, on the capillary number, Ca, is modelled in the literature by the (e) de Gennes (Gennes, 1985) and (f) Cox-Voinov (Cox, 1986; Voinov, 1976) models. (g) Contact angle dynamics in a vertically vibrating droplet and in (j) sloshing waves (snapshots over a period) (Viola, 2016). For these oscillatory flows, experiments by (h) Xia and Steen (2018) and (l) Cocciaro et al. (1993) suggest as suitable phenomenological contact angle laws the (i) nonlinear Dussan model (Dussan, 1979; Jiang et al., 2004), sometimes simply approximated by the (m) Hocking linear law (Hocking, 1987) supplemented with hysteresis.

contact line has been estimated by introducing, in the same spirit of Li et al. (2019), an intermediate boundary condition that assumes a linear relation between the contact line speed and slope, $\partial\eta/\partial n \propto \partial\eta/\partial t$ (Hocking, 1987), with a proportionality constant, sometimes referred to as mobility parameter M (Xia and Steen, 2018), that in our study has been kept constant in time. We note that, according to the linear relation,

$$\frac{\partial\eta}{\partial n} = M\frac{\partial\eta}{\partial t} \quad \text{mixed condition,}$$

the limiting values $M \to 0$ and $M \to \infty$ would correspond, respectively, to free-end and pinned-end edge contact line conditions. The agreement with experiments was found to be fairly good, although this proportionality constant was used as a fitting parameter.

With these simple contact line models, the damping of the system is assumed to have linear origins. Nevertheless, these assumptions altogether, by overlooking the actual nonlinear contact line dynamics, have led to a considerable underestimation of the actual overall dissipation in most of the small-size lab-scale experiments (Benjamin and Ursell, 1954; Henderson and Miles, 1990), for which the complexity of the region in the neighbourhood of the moving contact line, where molecular, boundary layer and macroscopic scales are intrinsically connected, is of extreme importance.

In order to understand and quantify better, at least from a macroscopic perspective, this extra dissipation, it is necessary to look more carefully at the dynamics of the oscillating contact line and at its wetting conditions, a long-standing problem in fluid mechanics that dates back to Navier Navier (1823) (see also Davis (1974); Eggers (2005); Eral et al. (2013); Huh and Scriven (1971); Keulegan (1959); Lauga et al. (2007); Miles (1990); Ting and Perlin (1995)).

When a liquid meniscus flows over a dry solid substrate, there is a triple-phase interface (air-liquid-solid), which experiences a complex nonlinear dynamics. For instance, let us consider two scenarios of uni-directional flows: a droplet sliding down with velocity U on an inclined dry plate in partial wetting conditions (see figure IV.1(a)); an expanding or contracting (at velocity U) liquid droplet (see figure IV.1(d)). Experimental observations (Dussan, 1979; Grand et al., 2005; Rio et al., 2005) have shown that the dynamic advancing, θ_a, and receding, θ_r, contact angles deviate from their static values depending on the velocity of displacement of the advancing or receding meniscus. Moreover, there exists a range $\theta \in [\theta_r, \theta_a]$ within which the contact line seems to remain stationary. The existence of such a static range, defined as contact angle hysteresis, plays a critical role in the nonlinear damping and dynamics of capillary-gravity waves.

Several models have been suggested to explain the relation between the dynamic contact angles, θ, and the capillary number defined by the drop velocity, U, i.e. $Ca = \mu U/\gamma$, with γ and μ, the air-liquid surface tension and dynamic viscosity, respectively. One such model for these uni-directional flows has been established by Gennes (1985), who extended to partial wetting conditions the Tanner law, originally derived in total wetting. This law connects the dynamic contact angles θ and the static (equilibrium) angle θ_s with the capillary number Ca. More precisely, the force required to draw the liquid is represented by $\gamma(\cos\theta_s - \cos\theta)$, while the viscous force is proportional to $\mu U\theta^{-1}\log\left(l_{macro}/l_{micro}\right)$. Here, l_{macro} denotes a macroscopic

characteristic length and l_{micro} is a microscopic cut-off length, which is necessary to prevent stress singularity, as pointed out by Snoeijer and Andreotti (2013). For small values of static and dynamic contact angles, the equation $\theta\left(\theta^2-\theta_s^2\right)=\pm 6Ca\log\left(l_{macro}/l_{micro}\right)$ holds true, with the ± signs that distinguish between the advancing and receding motion of the contact line.

Cox (1986) and Voinov (1976) arrived at a similar but different relation by solving lubrication equations for slightly curved air-liquid interfaces. Like the approach of de Gennes, their solution is truncated at both molecular and macroscopic scales, giving the law $\theta^3-\theta_s^3=\pm 9Ca\log\left(l_{macro}/l_{micro}\right)$.

In the study by Grand et al. (2005), it was noted that while certain models accurately depict the contact line dynamics observed in experiments, they fail to account for wetting hysteresis. As a result, when comparing these models to experimental data, the static contact angle θ_s is substituted with the limit static angle θ_a for the advancing branch and θ_r for the receding branch. Figure IV.1(e,f) displays the resulting $\theta(Ca)$ dependence for the de Gennes (e) and Cox-Voinov models (f), both of which incorporate a static hysteresis range Δ.

For oscillatory flows, the contact angle laws proposed in the literature share the same qualitative features as those derived for uni-directional flows, such as the *de Gennes* or the *Cox-Voinov* ones, but are described by quantitatively different relations. As this thesis focuses on oscillatory flows, the bottom part of figure IV.1 gives a brief overview of famous contact line models which have been used in this context. For instance, the contact angle dynamics observed for vertical vibrating sessile drops (figure IV.1(g)) or during the relaxation of sloshing waves (figure IV.1(j)) are seen to obey the nonlinear (cubic) *Dussan* model, $(\theta-\theta_s)^3\sim Ca$ (see figure IV.1(h,i)), and are sometimes well approximated by a modified *Hocking*'s law (supplemented with hysteresis, see figure IV.1(l,m)).

Furthermore, the rich dynamics of an oscillatory meniscus shows some interesting features that the next two Chapters of this thesis aim at reproducing and predicting. Those features are described in detail in figure IV.2. In a study conducted by Noblin et al. (2004), they investigated the behaviour of a water droplet on a solid surface with a finite contact angle hysteresis under vertical vibration (see figure IV.1(g)). The results showed two distinct types of oscillations. At low forcing amplitude, the contact line remains pinned (see figure IV.2(a)) and the drop displays eigenmodes at different resonance frequencies. At higher amplitudes, the contact line starts to move, remaining circular but with a radius oscillating at the excitation frequency. This transition between the two regimes occurs when the variations of the contact angle exceed the hysteresis range. They also observed a decrease in the resonance frequencies at larger vibration amplitudes for which the contact line is mobile. These features were attributed to the hysteresis acting as solid-like friction on the oscillations, leading to a stick-slip regime at intermediate amplitude (Dollet et al., 2020).

In his seminal works, Cocciaro et al. (1993, 1991) thoroughly characterized the contact angle dynamics during the natural (free-of-forcing) relaxation phase of the fundamental asymmetric sloshing mode in a small circular cylindrical container. Two different damping regimes were observed, corresponding to higher and smaller wave amplitude oscillations (see figure IV.2(b,c)). First, the contact line slides over the solid substrate experiencing progressive stick-slip transitions under the effect of the dynamic wall friction. In this phase, the damping

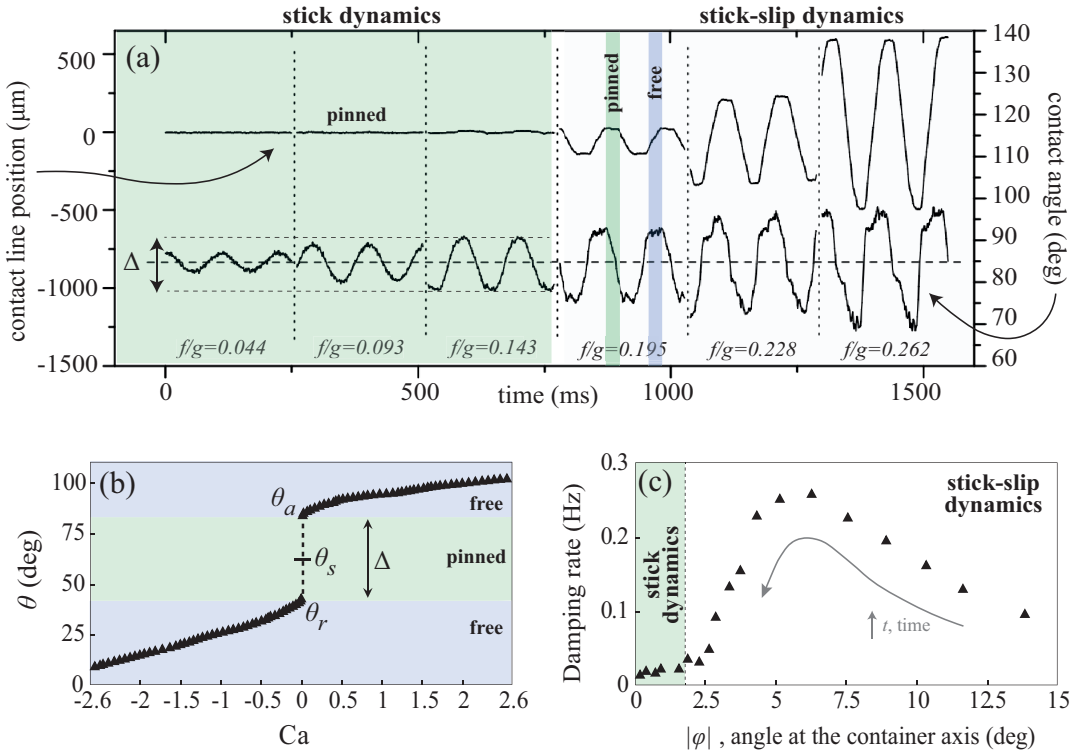

Figure IV.2 – (a) Transition between stick and stick-slip motions in a water sessile drop deposited on a vertically vibrating substrate characterized by a finite contact angle hysteresis ($\Delta \approx 10-15$ degrees) (Noblin et al., 2004). Lower curves are contact angle variations versus time, the dashed line represents θ_s. Higher curves are the contact line position around the starting position before vibrations. The six curves for different non-dimensional acceleration amplitudes f/g are joined together in the same plot for comparison. The driving frequency is $1/T = 9$ Hz. (b) Experimental contact angle dependence on the capillary number as measured by Cocciaro et al. (1993) during the natural relaxation dynamics of water oscillations in a cylindrical container initially perturbed using a loudspeaker, so as to induce the liquid motion. (c) Associated damping rate versus the amplitude of the angle measured at the container axis. The vertical dashed line indicates the value for which the contact line irreversibly pins.

increases considerably as the wave amplitude decreases, until it reaches a maximum value, after which it starts to decrease, and the small amplitude regime is established. A finite time of arrest for the contact line is found: the interface irreversibly pins and the following pure bulk motion is seen to decay exponentially owing to the linear viscous dissipation acting in the fluid bulk and in the Stokes boundary layers. The natural oscillations frequency initially matches the value associated with a free-end eigenmode, it increases during the decay, and it eventually tends to the value associated with a pinned-end eigenmode.

As an alternative to computationally expensive fully nonlinear direct numerical simulations (see (Amberg, 2022; Ludwicki et al., 2022) among others), different theoretical frameworks, attempting to rationalize the nonlinear dependence of the damping rate on the oscillation amplitude, have been recently proposed (Viola et al., 2018; Viola and Gallaire, 2018). These

works are based on an asymptotic formulation of the full hydrodynamic problem, which is tackled in the spirit of the weakly nonlinear and multiple timescale approach Stuart (1960), under precise assumptions and range of validity. The asymptotic analysis is found to be able to quantitatively predict the nonlinear trend of the damping in the higher amplitudes regime and the existence of a finite-time of arrest for the contact line, in agreement with experiments (Cocciaro et al., 1993; Dollet et al., 2020). However, it fails in capturing the transient stick-slip motion and, most importantly, the transition to the small amplitude regime, when the interface pins but the fluid bulk keeps oscillating with a smaller amplitude motion following a purely pinned dynamics.

The purpose of **Chapter 9** is to provide a different theoretical approach, which overcomes the limitations of these asymptotic analyses, thus successfully solving the overall flow dynamics and enabling us to extract and highlight realistic flow features, yet keeping a low computational cost. To this end, we consider viscous liquid oscillations in an idealized two-dimensional container and subjected to an experimentally inspired nonlinear contact line model, to which the contact line is forced to obey. Using a piecewise time splitting of the nonlinear contact line law, we formalize a mathematical model based on successive projections between different sets of linear eigenmodes pertaining to each linear split-piece composing the contact line law.

This procedure allows us to formally account for all the nonlinear features of small-amplitude capillary-gravity waves induced by a nonlinear contact line law acting at the lateral wall of a rectangular basin and, in particular, to correctly solve the transition from a contact line stick-slip (or nearly stick-slip) regime to the pinned (or nearly pinned) one. Indeed, each projection, corresponding to each stick-slip transition, eventually induces a rapid loss of total energy in the liquid motion and contributes to its nonlinear damping.

The projection method formalized in Chapter 9 for an idealized two-dimensional flow configuration with triple contact points (rather than lines), is extended in **Chapter 10** to describe the more realistic situation of liquid oscillations in a U-shaped tube, as experimentally investigated by Dollet et al. (2020). A thorough quantitative comparison with these experiments shows that the projection method correctly captures the final stick-slip-to-stick transition, as well as the secondary fluid bulk motion following the arrest of the contact line, overlooked by previous asymptotic analyses.